AIAA JOURNAL
Vol. 48, No. 9, September 2010

Plasma Volumetric Effects on the Force Production of a Plasma Actuator

G. I. Font,* C. L. Enloe,† and T. E. McLaughlin‡
U.S. Air Force Academy, Colorado 80840

DOI: 10.2514/1.J050003

Dielectric barrier discharge plasma actuators are examined experimentally and computationally. Experimental temporal force measurements show that the plasma actuator produces two positive (accelerating) forces per ac cycle. While the plasma is ignited, the actuator experiences an accelerating force, and, when the plasma is extinguished, a decelerating force appears. This occurs twice during each ac bias cycle. In addition, while the accelerating force is approximately equal in magnitude and direction during each half of the ac cycle, the decelerating force is not. Navier–Stokes simulations of the neutral air flow with a prescribed plasma force reveal that the variation in the decelerating actuator force is consistent with structural changes in the plasma itself. These plasma structural changes alter the volume over which the plasma force is imparted to the air and, in turn, change the amount of air drag incurred by the wall jet created by the plasma. During each actuator bias cycle, 70–90% of the momentum supplied by the plasma actuator is destroyed by drag with the wall immediately after the plasma extinguishes.

Nomenclature

C_D	=	wall drag coefficient $= F_{\text{Drag}}/(0.5\rho V^2 A)$
F	=	net horizontal force on flow, N
H	=	height of plasma area, mm
L	=	length of plasma area, mm
T	=	time/bias period, nondimensional
V	=	total velocity, m/s
$V_{x\text{ave}}$	=	average x velocity, m/s
ω	=	angular frequency, rad/s

I. Introduction

ATMOSPHERIC pressure plasma discharges have been under intense study [1–3] for a number of years due to their ability to modify the flow field around an aerodynamic body. Among the uses demonstrated for these plasma discharges are drag reduction, lift enhancement, turbulence mitigation, and boundary layer transition modification. A schematic of a generic plasma actuator is shown in Fig. 1. It consists of two electrodes separated by a dielectric and displaced in the streamwise direction. An alternating voltage is applied to the electrodes with a frequency of 100–1000 s of Hz and thousands of volts in amplitude. This results in the creation of a plasma over the top of the buried electrode which imparts a net downstream force onto the air.

Numerical and analytic models for the physics occurring in these plasmas have been undergoing continuous improvement but have not had quantitative experimental data, with the exception of the measurements of some average quantities, to compare against. Recently, however, advancements in experimental techniques have allowed the temporal measurement of flow velocity, force production, and surface charging [4–6]. These have, at last, provided data to allow direct detailed comparison and validation of computational results.

Presented as Paper 2009-4285 at the 39th AIAA Fluid Dynamics Conference, San Antonio, TX, 22–25 June 2009; received 16 June 2009; revision received 8 March 2010; accepted for publication 27 May 2010.

*Professor, Department of Physics. Member AIAA.
†Professor, Department of Physics. Senior Member AIAA.
‡Director, Aeronautics Research Center, Department of Aeronautics. Associate Fellow AIAA.

One recent experimental study [7] indicated that the force produced during the different halves of the bias cycle, while being similar in magnitude, produce significantly different levels of net (useful) momentum addition to the air. Several previous experimental and computational studies suggested [8–11] that the plasma structure was different during each half of the bias cycle. Among the differences noted, the volume and location of the plasma was found to be different during each half of the bias cycle. The present study attempts to ascertain if this is the reason for the differing net momentum addition to the air. The study is carried out by inserting plasma simulation results into a Navier–Stokes neutral gas simulation. Sec. II will review the experimental findings. Sec. III will briefly detail the computational method. Sec. IV will present the results followed by a summary and conclusions.

II. Review of Experimental Force Measurements

A recent experimental study, fully detailed in [7], measured the angular position of a torsional pendulum on which two plasma actuators had been mounted. Using a laser interferometer, displacements smaller than 100 nm were able to be measured. By carefully crafting the pendulum such that the restoring torque was a factor of 10–100 times smaller than the plasma torque and utilizing a small ac bias frequency (200 Hz), the temporal force characteristics of the plasma actuator were extracted directly from the motion of the system.

Figure 2 is reproduced from [7] and shows the angular velocity as a function of time and voltage for a typical experimental run. During each ac cycle, the pendulum accelerates twice and decelerates twice. Numerous previous experimental studies ([12], for example) have also shown that the plasma ignites twice during each ac cycle. The community has been debating, for some time, the direction of the force during each half of the ac cycle [13–15]. Specifically, the debate centers about whether the plasma pushes during each half cycle or whether it pushes during one half cycle and pulls during the other. Within the limits of the current experiments conducted in air, the answer is clear: during both the negative and the positive half cycle, the plasma force is accelerates the air downstream. Therefore, the plasma operates in a push-push mode. An explanation for this was proposed by a recent computational study [10] which suggested that a negative ion cloud builds up over the actuator during the forward stroke resulting in a downstream force.

Figure 3 displays the angular velocity as a function of time for a single ac cycle in order to compare the relative contributions to the force of each part of the ac cycle. Also, displayed in the figure is the driving voltage and the portion of the period when plasma is experimentally observed to be present over the actuator. While the

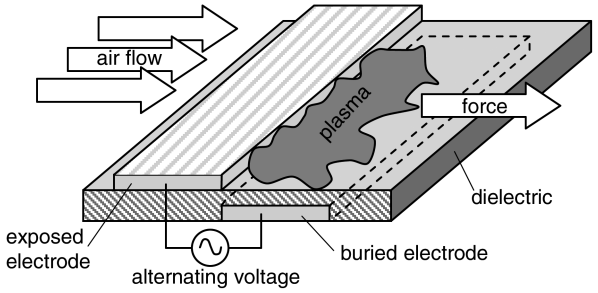

Fig. 1 Plasma actuator configuration.

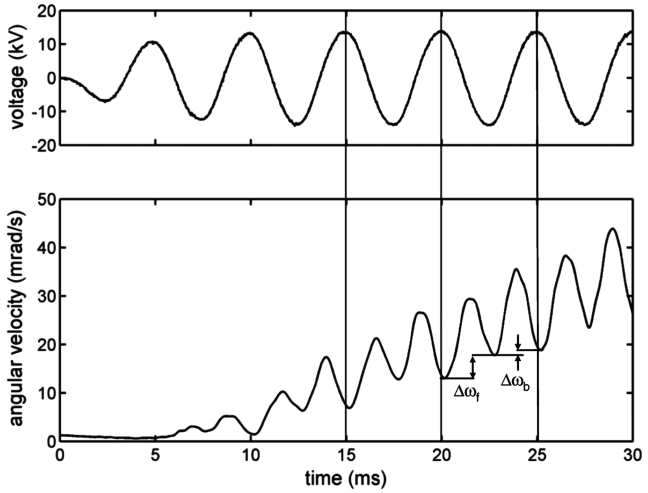

Fig. 2 Angular velocity of torsional pendulum as a function of time. Both positive and negative accelerations occur twice during each ac cycle of the discharge (from [7]).

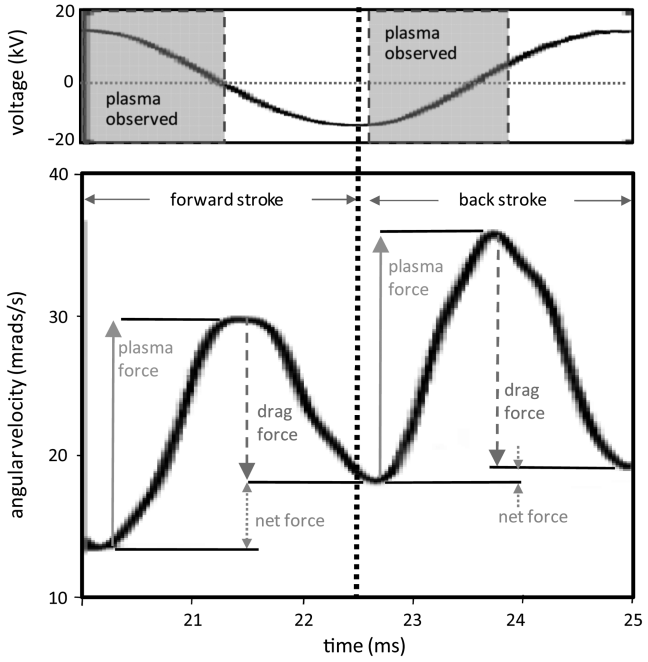

Fig. 3 Angular velocity as a function of time for a single typical ac cycle. The plasma force is proportional to the change in angular velocity. While the plasma force is comparable during the forward and back strokes, the drag is larger during the back stroke resulting in a smaller net force imparted to the air.

plasma is ignited a downstream force is imparted onto the air during both halves of the ac cycle. This again points out that the actuator is operating in a push-push mode. The force is nearly equal for both the forward and the back half of the ac cycle resulting in a comparable increase in angular velocity. Once the plasma extinguishes (from about 21.5–22.5 and 24–25 ms), the pendulum angular velocity diminishes. Detailed analysis shows that the pendulum is slowing down at a rate which is 10–40 times greater than can be attributed to the pendulum's restoring torque. Since the plasma is no longer present, this deceleration can not be attributed to electric forces either. A candidate for a decelerating force may be the shear force between the accelerated air over the actuator and the actuator surface. The first goal of the computational part of this study will be to try to ascertain if this is a real possibility.

Another important conclusion of the experiments was that the net force is larger during the forward stroke (negative going exposed electrode) than during the back stroke (positive going exposed electrode). This is shown in Fig. 2 as the net change in angular velocity, $\Delta\omega$. The experimental data in Fig. 3 shows that the drag force on the pendulum is greater during the second half of a typical ac cycle when compared with the first half of the ac cycle. Experimental and computational studies [7–9] have shown that the plasma structure can be different during each half of the ac cycle. Specifically, the volume and location of the plasma change as the structure changes. The second goal of the computational part of the study will be to explore whether the structural changes in the plasma can account for the drag differences during the first and second halves of the ac cycle.

III. Computational Method

In this study, a commercial neutral fluid Navier–Stokes code, FLUENT, was used to explore the response of the air to the force imparted by the plasma. The code has been documented exhaustively (for example [8,16–18]) and will not be discussed further here. The plasma force data is taken from previous simulations [8] and entered as a temporally and spatially varying momentum source term into the neutral fluid simulations. A similar technique was used in a previous study [19]. That study addressed momentum and heat addition by the plasma into the air but did not consider the plasma volume changes.

The domain and boundary conditions used for exploring the air response to the plasma force are shown in Fig. 4. The computations are done in two dimensions on a small region 10 by 5 cm. The domain size should be sufficient to capture the air response since the plasma length is typically less than 1 cm and the height is measured in tenths of millimeters. The computational results show that the domain is sufficiently large to reproduce experimentally observed vortex formation and subsequent vortex lift off the wall surface. Therefore, the domain size appears adequate for studying the air response in the immediate vicinity of the plasma actuator. The plasma forcing region is placed 1.5 cm from the edge of the domain. A symmetry boundary is immediately in front and behind the wall surface which is 9 cm long. Left and right boundaries are treated as pressure boundaries. The pressure difference between the inlet and the outlet is set at a few Pascal in order to give an initial velocity of about 0.1 m/s. This initial velocity is enough to stabilize the solver and still remain well below the plasma induced velocities which are typically above 5 m/s. The

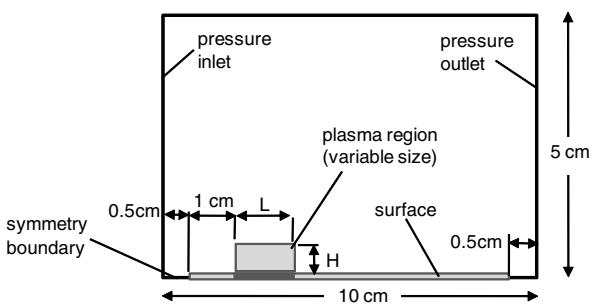

Fig. 4 Computational domain and boundary conditions used for exploring air response to plasma force.

top of the domain is treated as a symmetry boundary to improve the stability of the simulation. The computational mesh is a 7000 cell unstructured grid. It was refined and made more dense using velocity gradients until the shear layer and plasma regions had more than 30 cells in the direction perpendicular to the wall. A grid sensitivity study was undertaken where the grid density was roughly doubled. Since the results did not change in character, the smaller 7000 cell grid was used for the rest of the study. The study was also repeated using several different turbulence models and simple laminar formulation. The results did not change significantly for the low flow velocities employed in this study.

To simulate the plasma force, a momentum source term is added to the momentum conservation equations. This term is zero everywhere except inside the plasma region of the computational domain. The plasma force in this region is set to 2.0×10^4 N/m^3, which is typical value in these plasmas. This value is modulated during the simulation to reproduce the time-varying force which is present only while the plasma is on. In this study, the force is switched on and off in as a square wave. No attempt is made to model the force build up during plasma ignition and force decrease as the plasma decays. As mentioned above, experimental and computational studies have shown that the plasma structure changes when the voltage reverses during the ac cycle. This is illustrated in Fig. 5 which shows the ion number density during the two halves of the ac cycle, as computed in [8]. Consistent with experimental measurements, when the exposed electrode is negative, the plasma is diffuse and spread out. When the exposed electrode is positive, the plasma can enter a filamentary (streamer) mode and remains thin. When the exposed electrode is negative, the bulk of the force producing region remains near the exposed electrode and extends farther off the surface, as discussed extensively in [8]. Conversely, when the exposed electrode is positive, the high density force producing region is confined near the moving head of the streamer and remains closer to the surface. It is theorized that, when the plasma is filamentary, thinner, or closer to the surface, it will lose more of the momentum it imparts to the shear stresses at the wall surface. Conversely, when the plasma is diffuse, less of the imparted momentum will be lost to the shear with the wall when the plasma extinguishes.

The change in plasma structure can be modeled in the neutral fluid simulations by changing the height, H, and length, L, of the plasma region. While the plasma is ignited and the exposed electrode is negative, the length of the plasma region, L, will be 5 mm and the height, H, will be 0.5 mm. When the exposed electrode is positive, the length, L, will be 5 mm, and the height, H, will be 0.25 mm, in order to mimic the thinner plasma closer to the surface. The plasma force per volume will be adjusted during the simulation so that the total integrated force will be equal during both half-cycles. The actuator is assumed to be flush with the surface and no attempt is made to model the backward facing step of the exposed electrode. Since the height of this step is usually only about 0.1 mm, its effect on the neutral flow is assumed to be negligible.

IV. Results

The study was initiated by exploring the effects of a plasma which provided equal force throughout equal volumes during both halves of the ac cycle. The plasma region length, L, is set to 5 mm and the height, H, to 0.5 mm. The plasma force is 2.0×10^4 N/m^3 which is typical of these plasmas. The force is assumed to be directed parallel to the plate. No attempt is made to model the vertical component of the force in the present study. The solution was started by converging a steady state flow over a flat plate with a flow velocity of about 0.1 m/s. Time accurate computations were, then, initiated with the actuator providing a force in the plasma region during the parts of the ac cycle where the plasma is in existence (roughly during the first quarter and the third quarter of the ac cycle). Five to ten ac cycles are computed. Note that steady state is not sought because the experimental data were always taken during the initial plasma start up and not after it had been running for an extended time. The plasma force is included using a square wave input. No attempt is made to model the transient plasma density build up during the initiation of the discharge or the plasma density decay during its extinguishment.

Figure 6 displays the velocity contours for typical run. Two instances during the first half of the ac cycle are shown: $T = 0.1$ when the plasma is ignited and $T = 0.4$ when the plasma has extinguished. The high velocity region created by the plasma force is observed to move downstream and away from the surface. The maximum velocity created is about 6 m/s. This is similar to what has been seen in PIV experiments and lends some confidence to the simulation.

Figure 7a shows the average x velocity in the domain as a function of time for two actuation periods for a case where the plasma total force and volume are equal during both halves of the ac cycle. It bears a striking resemblance to the velocity measurements shown in Fig. 2. While the plasma is on, the air and pendulum accelerate (in opposite directions) and while the plasma is off, both decelerate. The magnitude of the variation of the velocity of the air in the computation is much smaller, however, due to it being averaged over the entire solution domain. In addition, the shape of the air velocity variation is closer to a saw tooth shape due to the fact that the computational force is applied using a square wave function. The experimental force is related to the local electric field magnitudes and ion density distribution. Since the plasma grows during ignition and decays during extinction the experimental force variation is smoother.

Figure 7b shows the net force imparted to the computational flow field as derived from differencing the total momentum in the domain. Each time the plasma ignites, the net force is positive. Even with a square wave force input, it does not remain constant. This is because, as the flow accelerates, the drag force on the wall increases, resulting in a diminished net force. When the plasma is off, the net force is negative (drag). The magnitude of the drag force is also observed to decrease in time. This is most likely due to the velocity of the air decreasing. Note that for a prescribed force which is equal during both halves of the ac cycle, the velocity increments and net drag are equal

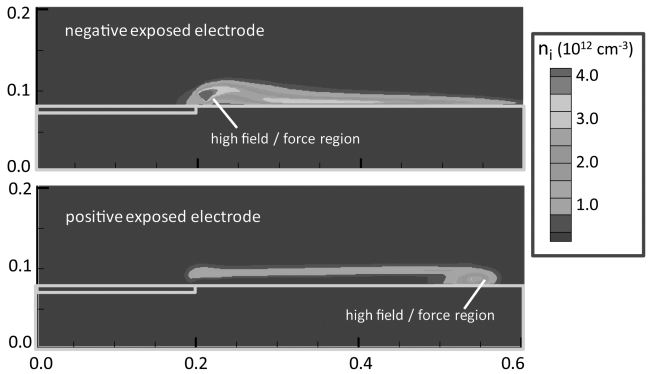

Fig. 5 Ion number density contours (cm^{-3}) during the two halves of the ac cycle. When the exposed electrode is negative the high density region of the plasma extends farther off the surface. When the exposed electrode is positive, the high density region of the plasma is thinner and closer to the surface (from [8], dimensions in cm).

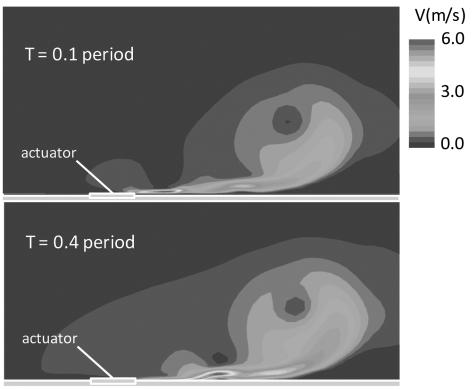

Fig. 6 Neutral flow velocity magnitude contours for the actuator during times in the ac cycle where the plasma is on ($T = 0.1$) and when the plasma is off ($T = 0.4$). The high velocity region created by the plasma force is observed to move downstream and lift off the surface.

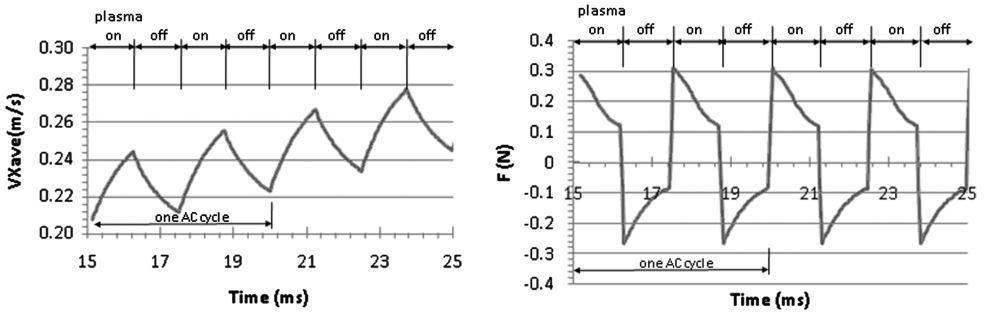

a) b)

Fig. 7 Effects on the flow field of a plasma actuator that imparts equal total forces over equal volumes during each half of the bias cycle: a) spatially averaged flow *X* velocity and b) net force (plasma and viscous) on the flow.

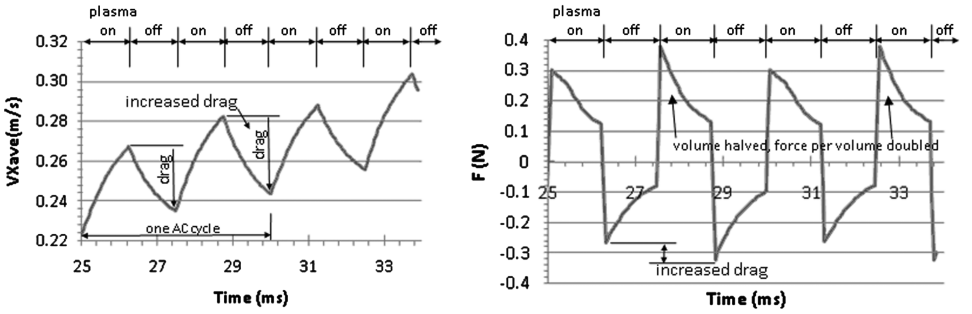

a) b)

Fig. 8 Effects on the flow field of a plasma actuator that imparts equal total forces during each half of the bias cycle, but where the volume during the second half is reduced by half. The reduction in plasma volume results in an increase in drag: a) spatially averaged flow *X* velocity and b) net force (plasma and viscous) on the flow.

during both parts of the cycle. Integrating the total force and drag shows that the 70% of the net positive momentum is subsequently destroyed by drag. Therefore, a very large part of the force being supplied by the actuator is being destroyed in the shear stress at the wall immediately after the plasma extinguishes. Experimental measurements of the average plasma actuator force are quantifying only about 10–30% of the force actually supplied by the actuator.

The time-resolved experimental measurements (Fig. 3) showed that while the plasma force appeared to be equal during both halves of the ac cycle, the net drag was not equal during each half cycle. One possible reason for this may be found in the plasma structural changes pointed out earlier. Perhaps while the total force is constant, the volume over which that force is deposited varies during the ac cycle. To explore this possibility, the neutral fluid computations were run where the volume of the plasma was altered during each half of the ac cycle. A plasma volume height, H, of 0.5 mm was used during the first half cycle and a height of 0.25 mm during the second half of the ac cycle. This imitates the observations of the plasma simulations that indicated a thinner plasma was formed closer to the surface during one half cycle of the discharge. The length of the plasma region, L, was maintained at 5 mm for both half-cycles and the plasma force per volume was doubled during the second half cycle in order to maintain the same total force for each half cycle. The results are shown in Fig. 8.

Figure 8 displays the average x (horizontal) velocity and net force imparted to the flow field as a function of time for two ac cycles when the plasma volume is reduced during the second half cycle. Figure 8a shows that the air continues to increase in velocity while the plasma force is present and decrease in velocity when it is removed. The decrease in plasma volume has the effect of making the magnitude of the decrease in velocity during the second half cycle larger. The drag is larger for the second half cycle. This is similar to what was observed in the experiments. The changes are easier to see in the total force imparted to the flow field displayed in Fig. 8b. When the plasma volume is cut in half and the force per volume is doubled, the drag on the air increases (as shown by the negative force at 29 ms when compared with the drag force at about 26 ms). Note that although the plasma force appears larger for the smaller volume, the time integrated total force between the two halves of the ac cycle are within 7% of each other. This small variation is due to grid discretization.

The amount of drag at the surface is quantified by Fig. 9 which displays the drag coefficient at the surface as a function of time. Each time the volume is reduced, the integrated drag at the wall increases by about 50%. This is due to higher velocities induced near the surface by the plasma which, during those parts of the ac cycle, have double the force per volume. Therefore, although the plasma is providing the same time integrated force for each half of the ac cycle, when that force is delivered over a smaller volume, more of it is lost due to drag. This results in a smaller net force applied to the air which is consistent with observations from the experiments. For this case, about 80% of the momentum supplied by the plasma actuator is destroyed in the surface drag immediately after the plasma extinguishes.

To confirm this behavior, the computations were repeated where, during the second half of the ac cycle, the volume was increased by a factor of two and the force per volume was halved. The resulting net force imparted to the flow field and the surface drag coefficient as a function of time are shown in Fig. 10. Imparting the plasma force over a larger volume decreases the net integrated drag force on the air by 30%, as shown in Fig. 10a. This is largely due to a decrease in wall drag during the second half of the ac cycle as shown in Fig. 10b. Note

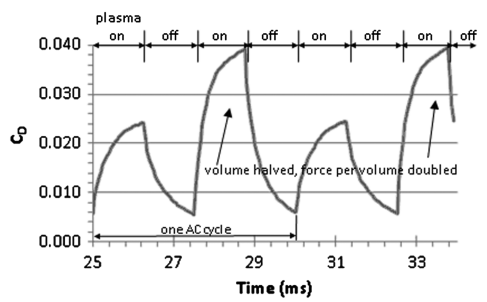

Fig. 9 Computed wall drag coefficient as a function of time for two ac cycles. The plasma volume is cut in half while the total force is constant during the second half cycle. The surface drag increases when the plasma volume is reduced.

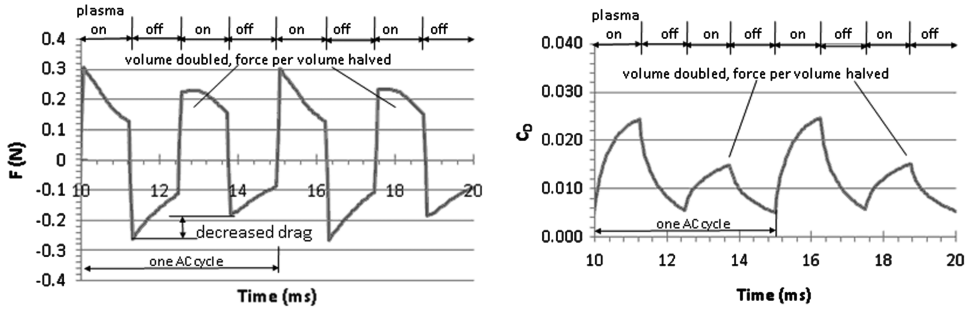

a) b)

Fig. 10 Effects on the flow field of a plasma actuator that imparts equal total forces during each half of the bias cycle, but where the volume during the second half is increased by a factor of two in the direction normal to the wall. The increased plasma volume away from the wall results in a reduction in drag: a) net force (plasma and viscous) on the flow and b) computed wall drag coefficient.

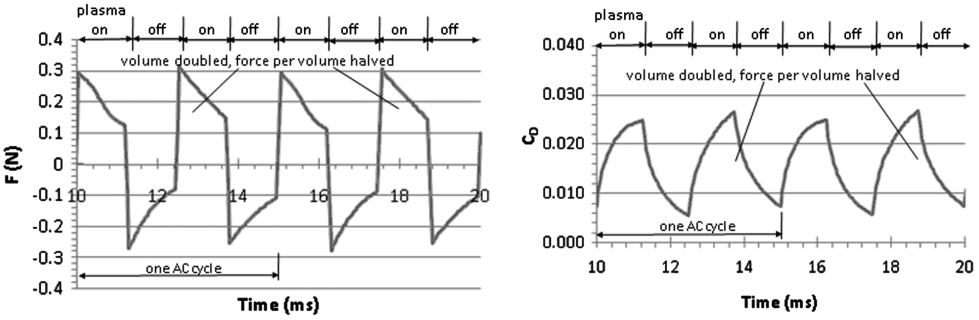

a) b)

Fig. 11 Effects on the flow field of a plasma actuator that imparts equal total forces during each half of the bias cycle, but where the volume during the second half is increased by a factor of two in the direction along the wall. The increased plasma volume along the wall does not result in a drag reduction: a) net force (plasma and viscous) on the flow and b) computed wall drag coefficient.

that although the positive plasma force appears different during each half cycle (compare force imparted at 13 vs 15 ms in Fig. 10a), the time integrated total force is within 1% of each other. Therefore, this confirms that the effectiveness of the actuator improves as the volume of the plasma increases.

A question arises at this point. Is the increase or decrease in drag truly related to the change in volume, a question of efficiency or turbulence losses, or is it related to the proximity of the wall, a question of surface shear stresses? To answer this question, a final simulation was run where the plasma volume was increased during the second half of the ac cycle, but the volume was maintained near the surface. For this simulation, the height, H, of the plasma was maintained at 0.5 mm, but the length, L, was increased from 5 to 10 mm during the second half of the ac cycle. Presumably, if it simply a question of efficiency and turbulence losses, the larger plasma volume will still yield the drag improvement of the earlier simulations with a volume increase. If, instead, the surface shear is more important, the new configuration with the larger volume should not yield an improvement in drag.

Figure 11 shows the resulting net force imparted to the flow field and the surface drag coefficient as a function of time when the plasma volume is increased but maintained near the wall during the second half of the ac cycle. Figure 11a reveals that the increase in plasma volume does not result in a large change in the net force (positive or negative) imparted to the flow field between the first half and second halves of the ac cycle. This is emphasized by the results for wall drag, shown in Fig. 10b, which also show little change between the different halves of the ac cycle.

Because of grid discretization, the time integrated positive plasma force for this case varies by about 10% between the half-cycles. Therefore, the 6% increase in the integrated drag is not significant. Nevertheless, the message is clear: increasing the plasma volume does not result in a decrease in drag unless the volume increase is away from the surface. The dominant loss of momentum for a plasma actuator appears to be the surface shear stresses and not the shear losses away from the surface. This result is consistent with research in near-wall jets.

V. Conclusions

Experiments quantifying the temporal force distribution from a plasma actuator have shown that the plasma accelerates the flow twice during each ac cycle. This supports a *push–push* characterization of the force from a plasma actuator. During each half of the ac cycle, while the plasma is ignited, the force is always directed downstream. Immediately after the plasma is extinguished, the force is directed upstream. The accelerating force is approximately equal between halves of the ac cycle, while the decelerating force after the plasma extinguishes is not equal. This study was conducted to explore why the decelerating force exists when the plasma is off and possible reasons behind the differences in the decelerating force. Navier–Stokes simulations of the neutral fluid with a spatially and temporally prescribed plasma force have revealed the following:

1) The decelerating force observed in the experiments after plasma extinction can be explained with simple fluid drag.

2) A large part of the force imparted by the actuator on the air (70–90%) is lost to the drag of the air with the adjacent wall surface almost immediately after the plasma extinguishes.

3) The changes in decelerating force observed in the experiments between different halves of the ac cycle can be explained by structural changes in the plasma which result in changes of the volume of the plasma over which the force to the air is deposited and the proximity of that volume to the surface.

4) When the plasma force is deposited closer to the surface, the wall drag increases resulting in less net force imparted to the air.

5) Force imparted by the plasma over a larger volume should result in lower drag losses if the increase in plasma volume is away from the surface.

References

[1] Roth, J. R., Sherman, D. M., and Wilkinson, S. P., "Electrohydrodynamic Flow Control with a Glow-Discharge Surface Plasma," *AIAA Journal*, Vol. 38, No. 7, 2000, pp. 1166–1172. doi:10.2514/2.1110

[2] Post, M. L., and Corke, T. C., "Separation Control Using Plasma

Actuators: Dynamic Stall Vortex Control on Oscillating Airfoil," *AIAA Journal*, Vol. 44, No. 12, 2006, pp. 3125–3135. doi:10.2514/1.22716

[3] Moreau, E., Louste, C., Artana, G., Forte, M., and Touchard, G., "Contribution of Plasma Control Technology for Aerodynamic Applications," *Plasma Processes and Polymers*, Vol. 3, No. 9, 2006, pp. 697–707. doi:10.1002/ppap.200600059

[4] Forte, M., Jolibois, J., Pons, J., Moreau, E., Touchard, G., and Cazalens, M., "Optimization of a Dielectric Barrier Discharge Actuator by Stationary and Non-Stationary Measurements of Induced Flow Velocity: Application to Airflow Control," *Experiments in Fluids*, Vol. 43, No. 6, 2007, pp. 917–928. doi:10.1007/s00348-007-0362-7

[5] Enloe, C. L., McHarg, M. G., and McLaughlin, T. E., "Time-Correlated Force Production Measurements of the Dielectric Barrier Discharge Plasma Aerodynamic Actuator," *Journal of Applied Physics*, Vol. 103, No. 7, 2008. doi:10.1063/1.289659

[6] Enloe, C. L., McLaughlin, T. E., Gregory, J. W., Medina, R. A., and Miller, W. S., "Surface Potential and Electric Field Structure in the Aerodynamic Plasma Actuator," AIAA Paper 2008-1103.

[7] Enloe, C. L., Mcharg, M. G., Font, G. I., and McLaughlin, T. E., "Plasma-Induced Force and Self-Induced Drag in the Dielectric Barrier Discharge Aerodynamic Plasma Actuator," AIAA Paper 2009-1622, 47th AIAA Aerospace Sciences Meeting, Orlando, FL, Jan. 2009.

[8] Orlov, D. M., Font, G. I., and Edelstein, D., "Characterization of Discharge Modes of Plasma Actuators," *AIAA Journal*, Vol. 46, No. 12, 2008. doi:10.2514/1.37514

[9] Boeuf, J. P., Lagmich, Y., Unfer, Th., Callegari, Th., and Pitchford, L. C., "Electrohydrodynamic Force in Dielectric Barrier Discharge Plasma Actuators," *Journal of Physics D: Applied Physics*, Vol. 40, No. 3, 2007, pp. 652–662. doi:10.1088/0022-3727/40/3/S03

[10] Lagmich, Y., Callegari, Th., Pitchford, L. C., and Boeuf, J. P., "Model Description of Surface Dielectric Barrier Discharges for Flow Control," *Journal of Physics D: Applied Physics*, Vol. 41, No. 9, 2008. doi:10.1088/0022-3727/41/9/095205

[11] Hoskinson, A. R., Oksuz, L., and Hershkowitz, N., "Microdischarge Propagation and Expansion in a Surface Dielectric Barrier Discharge," *Applied Physics Letters*, Vol. 93, 2008. doi:10.1063/1.3039805

[12] Enloe, C. L., McLaughlin, T. E., VanDyken, R. D., Kachner, K. D., Jumper, E. J., and Corke, T. C., "Mechanisms and Responses of a Single Dielectric Barrier Plasma Actuator: Plasma Morphology," *AIAA Journal*, Vol. 42, No. 3, 2004, pp. 589–594. doi:10.2514/1.2305

[13] Corke, T. C., Enloe, C. L., and Wilkinson, S. P., "Dielectric Barrier Discharge Plasma Actuator for Flow Control"*Annual Review of Fluid Mechanics*, Vol. 42, Jan. 2010, pp. 505–529. doi:10.1146/annurev-fluid-121108-145550

[14] Roy, S., and Gaitonde, D., "Multidimensional Collisional Dielectric Barrier Discharge for Flow Separation Control at Atmospheric Pressures," AIAA Paper 2005-4631, 2005.

[15] Font, G. I., and Morgan, W. L., "Plasma Discharges in Atmospheric Pressure Oxygen for Boundary Layer Separation Control," AIAA Paper 2005-4632, 2005.

[16] Kim, S., Mathur, S., Murthy, J., and Choudhury, D., "A Reynolds-Averaged Navier–Stokes Solver Using an Unstructured Mesh Based Finite-Volume Scheme," AIAA Paper 98-0231, 1998.

[17] Mathur, S., and Murthy, J., "A Pressure-Based Method for Unstructured Meshes," *Numerical Heat Transfer*, Vol. 31, No. 2, 1997, pp. 195–215. doi:10.1080/10407799708915105

[18] Fluent User's Guide, Fluent Inc., Lebanon, NH, 2005.

[19] Font, G. I., Jung, S., Enloe, C. L., and McLaughlin, T. E., "Simulation of the Effects of Force and Heat Produced by a Plasma Actuator on Neutral Flow Evolution," AIAA Paper 2006-0167, Jan. 2006.

M. Visbal
Associate Editor